The CN($X\ ^2\Sigma^+$) + C_2H_6 reaction. Dynamics study based on an analytical full-dimensional potential energy surface.

Joaquin Espinosa-Garcia* and Cipriano Rangel

Área de Química Física and Instituto de Computación Científica Avanzada

Universidad de Extremadura, 06071 Badajoz (Spain)

*E-mail: joaquin@unex.es

ABSTRACT

The hydrogen abstraction reaction of the cyano radical with molecules of ethane presents interest in the chemistry from ultra-cold to combustion environments, especially with regard to HCN(v) product vibrational distribution. In order to understand its dynamics a new analytical full-dimensional potential energy surface was developed, named PES-2023. It uses a combination of valence bond and mechanic molecular terms as functional form, fitted to high-level *ab initio* calculations at the explicitly correlated CCSD(T)-F12/aug-cc-pVTZ level on a reduced and selected number of points describing the reactive process. The new surface showed a continuous and smooth behaviour, describing reasonably the topology of the reaction: high exothermicity, low barrier and presence of intermediate complexes in the entrance and exit channels. Using quasi-classical trajectory calculations (QCT) on the new PES-2023, a dynamics study was performed at room temperature, with special emphasis on the HCN(v_1,v_2,v_3) product stretching and bending vibrational excitations, and the results compared with the experimental evidence, which presented discrepancies in the bending excitation. The available energy was mostly deposited as HCN(v) vibrational energy, with the vibrational population inverted in the CH stretching mode and not inverted in the CN stretching and bending modes, thus simulating the experimental evidence. Other dynamics properties at room temperature were also analysed; cold rotational energy distribution was found, associated with a linear and soft transition state, and backward scattering distribution, associated with a rebound mechanism.

1. INTRODUCTION

The gas-phase reaction between the cyano radical and the ethane molecule presents some interesting points for theoretical study: i) It is an exothermic reaction, with a low barrier height (even barrierless), which appears "early" on the reaction path, i.e., close to the reactants; ii) It presents a heavy-light-heavy mass combination (HLH) with a linear transition state, and a small skew angle, $\beta = 15.2^{o}$, β being the angle between the entrance and exit channels in mass-weighted coordinates. As a consequence of this kinematic condition the dynamics is governed by corner cutting on the skewed potential energy surface and two important effects appear: firstly, a priori, at low temperatures tunnelling should play a significant role, although in this particular reaction with a very low barrier, this effect is negligible, and secondly, substantial vibrational excitation would be expected, especially in the triatomic product;[1-3] iii) The HCN(v) vibrational distribution presents controversies among different experimental groups. Bethardy et al.[4] found that the HCN(v_1,0,v_3) states (i.e., bendless excitation) are not initially populated, while Copeland et al.[5] and Morris et al.[6] previously reported noticeable excitation of the bending mode. In this case, the three vibrational modes of HCN are described as C-N stretch (v_1), bend (v_2), and C-H stretch (v_3), and are all IR active;[7] iv) A full-dimensional potential energy surface is not available for this reaction; and finally, v) Its interest in the chemistry of low and ultra-low temperature environments, in the chemistry of planetary atmospheres[8] and of interstellar clouds,[9,10] and also at high temperatures, in hydrocarbon fuel combustion processes (through the nitric oxide chemistry cycle).[11,12]

The attack of the cyano radical on the ethane molecule begins with the formation of a weak intermediate complex in the entrance channel, RC, which evolves to the saddle point, SP, representing a configuration with formation and breaking of bonds. In the exit channel, an intermediate complex is formed, PC, which evolves to the corresponding products, hydrogen cyanide and ethyl radical, with the following mechanism,

$$CN(X\ ^2\Sigma^+) + C_2H_6 \rightarrow RC \rightarrow SP \rightarrow PC \rightarrow HCN(v_1,v_2,v_3) + C_2H_5,\ \Delta H^o_{298} = -25.6\ \text{kcal mol}^{-1}$$

where the standard enthalpy of reaction (298 K) was obtained from the compilation (Active Thermochemical Tables) of heats of formation of the individual species.[13] While kinetically this reaction has been widely studied, both experimentally (see compilation in the NIST chemical kinetics database, from 1965 to 2013),[14] and theoretically,[15] the dynamics interest has been scarce,[4-6] and to the best of our knowledge, no dynamics

theoretical works have been reported. Copeland et al.[5] in 1992 and Morris et al.[6] in 1994, reported experimental studies at room temperature on the product HCN(v_1,v_2,v_3) vibrational populations, as an example of heavy–light–heavy hydrogen abstraction reactions, using time resolved infrared fluorescence. These authors found appreciable vibrational excitation of all the modes, i.e., pure stretches (CN, CH) and bending or combination of these vibrations. Later, in 1995, Bethardy et al.[4], using time-resolved infrared absorption spectroscopy at 294±2 K, reported results in disagreement with the previous measurements. They found that pure stretch and combination of stretching vibrations, HCN(v_1,0,v_3), for the ground-state bending vibrational state, are not initially populated, or the population is <1%. All experimental studies reported that given the high exothermicity of the reaction, many vibrational states appeared populated, each with a low population.

Given the scarce dynamics theoretical information and the experimental controversies about the HCN(v_1,v_2,v_3) vibrational populations, the main aims of the present work are two-fold. Firstly, to develop for the first time an analytical full-dimensional potential energy surface (PES) to describe the nuclei motions, and secondly, based on this PES, to perform an exhaustive dynamics analysis at room temperature, to simulate the experimental evidence, on the HCN(v_1,v_2,v_3) vibrational populations and other dynamics properties not experimentally reported. The present paper is organized as follows. In Section 2, an analytical full-dimensional surface was developed, named PES-2023. It is basically a valence bond functional augmented with molecular mechanic terms, VB-MM, depending on a series of adjustable parameters, which represents in a smooth and continuous way this reactive system with ten bodies and 24 degrees of freedom. The new surface was based on high-level electronic structure calculations to locate and characterize (using the vibrational frequencies) all stationary points and the reaction path: reactants, products, saddle point, with special attention to the intermediate complexes in the entrance and exit channels. This information represents the input data. This Section finishes with a comparison of several properties of the new surface with the benchmark information used as input, which obviously represents a self-consistency test. The computational dynamics details appear in Section 3, using quasi-classical trajectory calculations (QCT) and a normal mode analysis to obtain the HCN vibrational modes. In Section 4 the dynamics results are presented and compared with the experimental information. Finally, the main conclusions are summarized in Section 5.

2. POTENTIAL ENERGY SURFACE: INPUT DATA, FUNCTIONAL FORM AND FITTING.

In general, all development of PESs begins with an extensive number of electronic structure calculations describing the reactive system, which represents the input data. In the VB-MM framework, the process continues with the proposition of different functional forms describing typical nuclei motions in the reactive system, stretching, bending in the plane and out-of-plane, torsions etc., which depend on a set of adjustable parameters. The process finishes with the fitting of these parameters to the input data.

The input data represents the first step in this process. All stationary points (reactants, products, intermediate complexes and saddle point) were located (geometry optimization) and characterized (vibrational frequencies, where the first points were characterized by positive values, while the saddle point presents only one imaginary frequency) using high level *ab initio* calculations, coupled-cluster with single, double and triple (perturbative) excitations with basis sets of triple-zeta quality, CCSD(T)/cc-pVTZ. At this level, it is important to note that we found many difficulties in the location of the reactant complex in the entrance channel and we assume that they are related with the flatness of the PES in this region. Finally, to improve the energetic description, the single-point technique was used, i.e., based on previous optimized geometries, the energy is improved using the explicitly correlated method with a larger basis set, CCSD(T)-F12/aug-cc-pVTZ. The *ab initio* calculations were performed using the Gaussian16[16] and Molpro[17] codes.

Given the presence of the CN radical, a high multi-reference character was previously[15] noted, which presents a high Q1 diagnostic,[18] 0.068 and 0.033 for the CN radical and the saddle point, respectively. The Q1 diagnostic in QCISD(T) calculations is the equivalent to the T1 diagnostic in CC calculations.[18,19] In the original paper[18] it was reported that in general the Q1 diagnostic overestimates the multi-reference character, Q1 > T1, which demonstrates that as the nondynamical correlation becomes more important, the QCISD results deteriorate faster than the CCSD ones. It is known[19] that T1 values greater than 0.02 for closed-shell or 0.045 for open-shell systems suggest that a multi-reference method might be needed. In the present work, based on the saddle point geometries optimized at the CCSD(T)/cc-pVTZ level, the T1 diagnostic gives values of 0.051 for the CN radical and 0.029 for the saddle point, showing that a single-reference method could be suitable, although obviously it is a limit case.

In addition to the stationary points, the reaction path from reactants to products was also calculated. However, due to the very high computational cost of the CCSD(T)-F12a/aug-cc-pVTZ level and our computational limitations, we explored more economic alternatives, second order Møller-Plesset perturbation theory, MP2/6-31G(d,p). At this low level, we began by locating and characterizing all the stationary points. Next, starting from the saddle point, the reaction valley was constructed using 50 points, calculating energy, gradient and Hessian matrices at each point between s=-3.0 bohr (in the reactant side) and s=+3.0 bohr (in the product side), where the reaction coordinate, s, is defined as the signed distance from the saddle point, s = 0. So, we describe the reaction path and orthogonal motions at these 50 points. In numerical terms, the Hessian matrix represents a 30x30 matrix, corresponding to 10 atoms times 3 Cartesian coordinates, in total 900 energies per point, and since 50 points were calculated, this effort is equivalent to about 45 000 energy calculations. Note, however, that at the MP2 level fortunately the second energy derivatives are analytical, which is equivalent to a noticeably lower computational effort. As a simple test of quality of this method, we compared some properties of the stationary points with the most accurate CCSD(T)-F12/aug-cc-pVTZ single-point calculations. The MP2 method gives a reaction energy of -40.45 kcal mol^{-1} as compared to -23.12 kcal mol^{-1} at the highest level, and a barrier height of +0.31 kcal mol^{-1} as compared to +0.21 kcal mol^{-1}. Clearly, the energetic description must be improved. Therefore, at 20 points on the reaction path, single-point calculations at the CCSD(T)-F12/aug-cc-pVTZ level on the MP2 geometries were performed. With this approach, the reaction energy and barrier height were, respectively, -26.04 and 0.29 kcal mol^{-1}, simulating the highest level.

In recent years, our group has accumulated a wealth of experience in the development of surfaces for polyatomic systems based on valence bond functions augmented with molecular mechanic terms, VB-MM.[20-24] This type of surfaces presents some advantages with respect to other strategies: a) capability to describe the reaction based on physically intuitive terms associated with familiar nuclear motions (stretching, bending, torsion, etc.); b) transferability of the adjustable parameters from a previous surface to a new one; c) easy refit to fine-tune the PES using new *ab initio* data at selected points; d) capability to reproduce zones of the reaction that were not included in the fit, due to the flexibility of the functional forms to represent the nuclear motions and e) lower computational demand. For the title reaction, the full-dimensional PES was developed

based on recent research on the CN + CH_4 reaction[25] and the OH + C_2H_6 reaction.[22] From the former, we reused the parameters describing CN stretching for the reactant and the stretching and bending modes in the HCN product. From the latter, we reused the parameters describing the ethane molecule in reactants and the ethyl radical in products. Small modifications on these parameters based on the present input data permitted us to simulate the title reaction. In this sense, the strategy is reminiscent of the popular tetris puzzle game, i.e., to assemble a new building based on known pieces. A term-by-term detailed description can be found in our previous works,[22,25] so they are not presented here to avoid unnecessary repetitions. Basically, the VB-MM potential describing this ten-body reaction is expressed as the sum of six terms,

$$V = V_{str} + V_{CC} + V_{bending} + V_{op} + V_{tor} + V_{HCN} \quad (1)$$

The first two terms are related with stretching motions describing, respectively, the six equivalent C-H bonds and the C-C bond in ethane. V_{str} is developed as the sum of six London-Eyring-Polanyi functions while V_{CC} is described as a Morse function. They depend on 26 and 3 adjustable parameters, respectively. The following two terms describe bending motions associated with the ethane-ethyl transformation in the reaction. $V_{bending}$ is developed as the sum of harmonic terms, where the angles associated to hydrogen atoms bonded to C_1 and C_2 were separated to treat independently both methyl groups, equivalent in ethane, which evolve towards $–CH_3$ or $–CH_2$ non-equivalent groups in the ethyl product. This term depends on 22 adjustable parameters. V_{op} is developed as a quadratic-quartic potential and was included to reasonably simulate the change from the pyramidal ($-CH_3$ group) in the reactant to the planar ($-CH_2$ group) geometry in the product. Only 6 adjustable parameters were necessary to define this term. Another important nuclei motion in this reaction is related with the torsion around the C-C bond between the two methyl groups. To describe this motion, the V_{tor} term is included, which depends on 3 adjustable parameters, describing the torsional barrier height and the torsional angle in ethane. Finally, the V_{HCN} potential is included to describe the HCN product, depending on 6 adjustable parameters. This term includes the new CN stretching motion, which is defined as a Morse potential, and the HCN bending motion, which is described as a harmonic term taking as reference angle the lineal HCN (180º) structure. Note that the V_{HCN} term was developed to correctly describe the number of vibrational frequencies in the CN reactant (one) and HCN product (four, with degenerated bending modes). The six terms included in Eq. 1 give a very rigid description of this ten-body

polyatomic system. Therefore, several switching functions were included to relax the reactive system from reactants (cyano radical + ethane) to products (hydrogen cyanide + ethyl radical). These functions were developed as hyperbolic tangent functions, to ensure smooth changes as the reaction evolves and finally give great flexibility to the PES. In total, the new PES depends on 66 adjustable parameters.

The next step in the development of PES-2023 was the fitting process of the 66 parameters to the input data. In 2009, our group[26] developed a least-square method, which uses energies, gradients and Hessians to attempt to automatize the fitting process and to obtain the best set of parameters. However, when all parameters are included, the automatic process is unsuccessful, and finally a trial-and-error hand-made process is needed. Thus, the fitting process is divided in four iterative steps. The description of the reactant and product properties, such as geometry, vibrational frequencies and energy of reaction, represents the first, and simplest, step. For instance, the reaction energy is related with the difference of the dissociation energies for the formed and broken bonds, which are two adjustable parameters. The description of the saddle point is a delicate issue, and represents the second step. Here, we should pay special attention to the barrier height and the imaginary vibrational frequency, which is related with the curvature of the path in this stationary point. The following step is the description of the reaction path from reactants to products. Here, the falls to reactants (smooth) and products (pronounced) from the saddle point are simulated. This is a complicated and laborious process because of the asymmetry of the reactant and product valleys, which involves many parameters. Finally, the fourth step is the description of the intermediate complex properties in the entrance and exit channels. In the present reaction, this step represented a laborious task (specially the location of the complex in the entrance channel) because of the different stability of both complexes. Once these four steps were performed, we obtained the first iteration and the first set of the 66 adjustable parameters, which represents the first approximation to the problem. These steps must be iteratively repeated until a reasonable agreement with the input data is reached, obtaining thus the final set of parameters. Note that the process is tedious and a time-consuming task. In sum, the new surface, named PES-2023, presents a physically intuitive functional form (related to familiar nuclei motions), the first energy derivatives (gradients) are numerical, it is symmetric with respect to the exchange of the six hydrogen atoms in ethane, and finally, it depends on a reduced number of adjustable parameters. The new surface will be published in the online version[27] of POTLIB.[28]

This section finishes with a comparison with the input data, because the accuracy of a PES is measured by its ability to simulate the *ab initio* information used as input data, which is, basically, a self-consistency test. Figure 1 presents a schematic representation of the CN + C_2H_6 surface showing the comparison of the stationary-point relative energies (with respect to the reactants) obtained on the PES-2023 with the CCSD(T)-F12/aug-cc-pVTZ level used in the fitting. In general, the new PES-2023 surface reproduces the *ab initio* information. The hydrogen abstraction reaction is very exothermic, with classical reaction energy of -22.20 kcal mol^{-1} as compared to -23.12 kcal mol^{-1} at the *ab initio* level. When thermal corrections at 298 K were included, the standard enthalpies of reaction were, respectively, -25.55 and -25.32 kcal mol^{-1}, both reproducing the experimental value from the corresponding standard enthalpies of formation,[13] -25.6 kcal mol^{-1}. The saddle point description is very important because it represents a sensitive zone of the reactive process. PES-2023 gives a barrier height of 0.23 kcal mol^{-1}, reproducing the ab initio data, 0.21 kcal mol^{-1}. It presents a linear C-H'-CN configuration, where the length of the formed H´-CN bond, 1.793 Å, is greater than the broken C-H´ bond, 1.113 Å (H' being the transferred hydrogen) reproducing *ab initio* calculations (1.785/1.125 Å) and previous theoretical calculations[15] (1.797/1.133 Å). In this case, with respect to the reactants and products, the broken and formed bonds increase by 2 and 67% respectively, indicating a clear "early" transition state, i.e. it appears soon on the reaction coordinate, in the entrance channel, which is related with a very exothermic reaction. This behaviour has, obviously, dynamics consequences, as will be analysed later. The corresponding imaginary vibrational frequency, related with the low barrier height and associated with the curvature of the reaction path, is expected to be very low. The PES-2023 frequency is 150 i cm^{-1}, simulating the *ab initio* information, 196 i cm^{-1}, and another theoretical result,[15] 212 i cm^{-1}, related in that study with a higher barrier, 0.41 kcal mol^{-1}. Finally, PES-2023 correctly describes the presence of intermediate complexes in the entrance and exit channels. The reactant complex is stabilized by 0.27 kcal mol^{-1} with respect to the reactants, and the corresponding product complex by 1.10 kcal mol^{-1} with respect to the products. These stabilities are slightly lower than those obtained with *ab initio* results. The largest difference found corresponds to the geometric configuration of the reactant complex (see insert in Figure 1). So, while PES-2023 locates a linear C-H'-CN approach, the CCSD(T)/cc-pVTZ level locates a "quasi" cyclic structure. In this last case, we should emphasize that we had many problems of convergence in the optimization process (passing from minimum to saddle point configurations in some iterations of the process),

probably due to the use of numerical second energy derivatives at this *ab initio* level. Interestingly, using the popular DFT M08HX level[29] (Minnesota density functional theory) with the MG3S basis set[30] (equivalent to the 6-311++G(3d2f,2p) basis set) which uses analytical second energy derivatives, the cyclic structure was not found, although the approach was not linear either. At this level (with energy improved by single-point calculations at the CCSD(T)-F12/aug-cc-pVTZ level) the reactant complex is stabilized by 0.47 kcal mol^{-1} with respect to the reactants, in agreement with the previous results.

Figure 2 shows the minimum energy path (MEP), with the energy changes along the reaction path, for the PES-2023 and the *ab initio* input data at the CCSD(T)-F12/aug-cc-pVTZ//MP2 level. PES-2023 reasonably simulates the entrance channel, which is very flat and difficult to calculate, with the largest differences in the exit channel, about 2.5 kcal mol^{-1}. However, considering all points used in the fitting process, the overall root-mean-square error (RMSE) is 1.7 kcal mol^{-1}, which seems reasonable given the high number of degrees of freedom in this polyatomic system. A more stringent test was performed using geometries not used in the fitting and again comparing the energy obtained with PES-2023 and CCSD(T)-F12/aug-cc-pVTZ. We begin by calculating a scan of points, where the breaking C-H' and forming H'-CN bond lengths vary in the range 1.0-3.0 Å. These geometries correspond to energies in the range between +25 and -25 kcal mol^{-1}, i.e. a range of ~50 kcal mol^{-1}. On this scan, 10 randomly scattered geometries were selected for comparison. In this case, using points outside the points used in the fitting, the RMSE is slightly larger, 2.4 kcal mol^{-1}. This result seems reasonable given the wide range of energies used and proves the accurate and limitations of the new surface. Figure 3 (upper panel) presents the bi-dimensional contour plot using the PES-2023, where the breaking C-H' and formed H'-CN bonds are represented in the range 0.9-3.0 Å, the remaining coordinates being fixed in the saddle point. This contour plot covers all dynamically relevant zones for the reaction, from the entrance channel with the weak reactant complex to the very exothermic product channel with the stabilized product complex. In addition, it shows the smooth, continuous and differentiable behaviour of PES-2023.

Before finishing this Section, we consider it of interest to make a comparison with the "cousin" CN + CH_4 reaction, which will permit us to analyse the first alkanes of the series. In 2017 our group[25] developed an analytical potential energy surface, PES-2017, describing this gas-phase reactive process, and the results are presented here. Table 1

compares important properties for both reactions and Figure 3 (lower panel) also includes the contour plot for the methane reaction. The reaction of the CN radical with both alkanes shows a similar topology, with a weak complex in the entrance and a stronger complex in the exit channel. However, the reaction with methane presents a higher barrier (2.5 versus 0.23 kcal mol^{-1}) associated with a larger imaginary frequency at the saddle point and with a lower exothermicity. In consequence, the reaction with methane presents a thinner barrier, and a larger tunnelling contribution was observed,[25] which is practically negligible in the reaction with ethane. The small stability of the reactant complex, which produces a practically flat entrance valley, is due to the smaller dipolar moment of the CN radical, (1.450 Debye) as compared with the OH radical (1.668 Debye) in reactions with methane[21] and ethane,[22] which presented more stabilized intermediate complexes. Finally, it is interesting to emphasize the increase of the rate constants in the reaction of the CN radical in the series of alkanes: methane, ethane and propane:[14] at 298 K, respectively: $8.5.10^{-13}$, $2.9.10^{-11}$ and $5.5.10^{-11}$ cm^3 $molecule^{-1}$ s^{-1}. This tendency is associated with the barrier height, 2.5, 0.23 and ~0[31] kcal mol^{-1}, with the exothermicity, -20.0, -22.2 and -25.9[31] kcal mol^{-1} and finally with the weakening of the C-H bond in the series methane, ethane and propane:[13] 105.0, 101.0 and 101.4 kcal mol^{-1}.

3. THEORETICAL TOOLS: QUASI-CLASSICAL TRAJECTORY CALCULATIONS AND NORMAL MODE ANALYSIS.

Based on an accurate and full-dimensional PES, the state-to-state dynamics description at a quantitative level comparable to experiments would need full dimensional quantum mechanical (QM) calculations. However, for polyatomic systems this goal is far from being achieved because the calculations are computationally prohibitive. In this case, quasi-classical trajectory (QCT) calculations represent an interesting and computationally economic alternative, although their classical nature presents some limitations. Using the PES-2023 surface, QCT calculations were performed at room temperature, to compare with the experimental evidence.[4-6]

We begin with the initial conditions of the trajectories. QCT calculations on the PES-2023 surface were performed using the VENUS96 code.[32,33] Trajectories were propagated from an initial C-CN separation of 15 Å, and stopped when this distance was greater than 20 Å. These long distances entail long flight times and more computational

effort, but in this way we ensure that no interaction is present in the reactant and product asymptotes. The propagation step is 0.1 fs to ensure that the energy and angular moment are conserved along each trajectory. At 298 K we ran 100 000 trajectories, where the CN radical rotational and vibrational quantum numbers were fixed at the ground-state. The ethane vibrational and rotational energies were selected by thermal sampling to reproduce the 298 K thermal distribution, and the relative translational energy of the reactants was obtained from the $E/(RT)^2$ exp(-E/RT) distribution. The remaining initial conditions (impact parameter, spatial orientation and vibrational phases) were selected from a Monte Carlo sampling. The maximum impact parameter, b_{max}= 6.5 Å was determined using small batches of trajectories, until no reactive trajectories were found. Given the large number of trajectories run, the statistical error is small or negligible (< 2%), and so they are not shown in the results. QCT calculations have a classical nature and so some trajectories end with vibrational energy below their zero-point energy (ZPE). This issue is commonly known as the ZPE violation problem. In the present paper we contemplated two approaches: considering all reactive trajectories in the final analysis (All approach) or considering only reactive trajectories with vibrational energy of each product, HCN and C_2H_5, above their respective ZPEs (DZPE approach, double ZPE approach). The latter approach is physically more reasonable but it drastically reduces the number of reactive trajectories for the final analysis. In this case, the reactive trajectories, 3373, are reduced to 1192 when the DZPE constraint is applied.

The QCT outcome, which is formed basically by Cartesian coordinates and momenta at the end of each reactive trajectory, permits us to directly obtain a series of dynamical properties: vibrational and rotational energies of the HCN and C_2H_5 products, E^{vib}_{HCN}, E^{rot}_{HCN}, E^{vib}_{C2H5} and E^{rot}_{C2H5}; the scattering angle θ between the HCN product and the incident CN radical, and the relative translational energy, E_{trans}, between HCN and C_2H_5. However, the a_1-a_3 actions for the HCN(v_1,v_2,v_3) product, one of the main aims of the present paper, are not directly obtained from the QCT outcome; they were calculated using the normal mode analysis method developed in our group, NMA method.[34] These actions correspond to CN stretching (ν_1 = 2046 cm^{-1}), bending (ν_2 = 723 cm^{-1}, doubly degenerate) and CH stretching (ν_3 = 3527 cm^{-1}), respectively. The actions are real numbers and were rounded to their nearest integer, n_1-n_3, which corresponds to the standard binning approach, SB, i.e., each reactive trajectory contributes to the final result with weight unity. More sophisticated alternatives have been proposed, which carry

a higher computational cost: in the Gaussian binning approach, GB,[35,36] each reactive trajectory is weighted by a Gaussian function, so that the larger the weight the closer the action to an integer number. This approach is computationally very demanding, and the energy-based Gaussian binning approach,[37,38] 1GB, is an economic alternative, where the total vibrational energy of each product is quantized. These last two approaches (or a purely quantum treatment, when this is possible) are affordable and realistic when few product vibrational states are populated; however, this is not the case for the HCN(v_1,v_2,v_3) product in the title reaction, where many vibrational states are populated with low individual population (see below in Results), and in these conditions the SB approach is advisable. This good behaviour was found in previous studies for the CN + CH_4 → HCN(v_1,v_2,v_3) + CH_3 reaction[39] and for the OH + CO → H + CO_2(v_1,v_2,v_3) reaction,[40,41] where the CO_2 product also presented a large number of populated vibrational states, and where the SB and the more expensive 1GB approaches gave similar populations. A different picture was found when few vibrational states were populated. This is the case of the OH + D_2 → HOD(v_1,v_2,v_3) + D reaction,[42] where the 1GB approach improved the agreement with experiment.

4. RESULTS AND DICUSSION

We begin by analyzing product energy partitioning. At room temperature using the DZPE approach, the QCT/PES-2023 energy fractions as vibration, rotation and translation for both products, HCN and C_2H_5 are, respectively (in percentages): f_v^{HCN} = 65, f_R^{HCN} = 6, f_v^{ethyl} = 12, f_R^{ethyl} = 7 and f_{trans} = 10. Clearly, the largest fraction of energy is deposited as vibration energy of the HCN product, 65%, with few rotational excitations in both products. This is the expected behaviour in a very exothermic reaction with a heavy-light-heavy mass combination. The small fraction of energy deposited as vibration in the C_2H_5 co-product, 12%, suggests that this product will appear practically in its vibrational ground-state. This tendency is similar to that found for the CN + CH_4 reaction:[39] 52, 8, 15, 7, and 18%, respectively, (note that, strictly speaking, these values correspond to a fixed collision energy of 1.0 kcal mol^{-1})[39] showing that these reactions with alkanes present similar dynamic behaviour.

Before starting the analysis of the HCN product vibrational analysis, one of the main objectives of the present paper, we present a series of previous considerations. The total energy available to the products corresponds to the sum of the collision energy,

Ecoll, the 0 K enthalpy of reaction, and the C_2H_6 rotational energy. At 298 K the collision energy was obtained from an energy distribution (see Section 3) with the most probable values between 0.5 and 1.5 kcal mol^{-1}. Here, we assume an average value of ~1.0 kcal mol^{-1}. The C_2H_6 rotational energy was obtained by thermal sampling at 298 K, which adds on average 0.9 kcal mol^{-1}. The enthalpy of reaction at 0 K is -26.0 kcal mol^{-1}. Therefore, the energy available to products is ~ 28 kcal mol^{-1}. Taking into account this available energy and the HCN(v_1,v_2,v_3) vibrational frequencies, one must expect a high vibrational excitation in all vibrational modes, up to four quanta in the CN stretching mode, up to two quanta in the CH stretching mode and up to thirteen quanta in the bending mode. These values correspond to pure vibrational states, but obviously any stretching-bending combination is possible, compatible with the energy, for instance, (1,4,1). This high population of the three modes simulates the experimental evidence.[4-6] Figure 4 presents a schematic representation of the available energy and pure excited vibrational states for the HCN(v_1,v_2,v_3) product.

At 298 K on the QCT/PES-2023 results, the NMA analysis reported more than 300 populated HCN(v_1,v_2,v_3) vibrational states, and 150 states with population > 0.1 %, the most populated state, HCN(1, 0, 1), presenting a population of only 8%. This picture is similar to those obtained in our previous work on the CN + CH_4 reaction,[39] and they clearly show that these low populations will represent a challenge in experiments. Figure 5 presents the lowest bending vibrational states, which show practically Gaussian distributions of the bending mode (i). The population of the pure stretch and combination of stretching states and bendless excitation, HCN(v_1, 0, v_3) has been a debatable issue in the experimental literature.[4-6] While Copeland et al.[5] and Morris et al.[6] reported initial state population (although no quantitative information was reported), Bethardy et al.[4] found that they were not initially populated, or that at least the initial population in each of these levels was <1%. However, this result contrasts with that obtained by the same group[43] a year later for the CN + CH_4 reaction, in which about 20% of the HCN product was initially produced in the bendless HCN(v_1, 0, v_3) states which, a priori, is surprising because both reactions present similar dynamics. In the present theoretical study, we found a population of 22%, which agrees with Copeland et al. and Morris et al.'s results for the title reaction and with the results for the reaction with methane. In sum, all the results reported that the HCN product appears vibrationally excited in the bending states, the discrepancy remaining in the percentage. In order to explain the theory/experimental discrepancies different causes were analysed following the arguments developed in our

previous work where the description of water product in polyatomic OH + XH → H_2O + X (X ≡ D, Br, NH_2 and GeH_3) reactions was analysed.[44]

As a first factor to explain the bending excitation, Bethardy et al.[4,43] and Nizamov et al.[45] pointed out the relation with the bending potential of the NC…H…R geometry in the linear transition state, R≡ CH_3 or C_2H_5: soft transition states will yield more bending excitation. Now, we have quantitatively analysed this suggestion for the CN + methane and ethane reactions. Figure 6 shows the variation of the energy as a function of the NC…H'…R bending angle in the saddle point for both reactions using analytical surfaces from our lab, PES-2023, for the ethane reaction (present work) and PES-2017[25,39] for the methane reaction. Both reactions present similar behaviour, showing soft transition state structures, small dependence with the bending angle, and differences between them of only 0.05 kcal mol^{-1} at an angle deviation of 30º with respect to the saddle point geometry. In consequence, similar bending excitations would be expected in both reactions, and this is the behaviour found in our theoretical studies with methane and ethane, with only 10 % and 22%, respectively, of bendless states, i.e., the HCN product appears mainly with bending excitation. The second factor is coupling of vibrational modes and, therefore, transfer of energy between them, along the reaction path. Figure 7 shows the changes of the vibrational frequencies along the reaction path, where for a clearer presentation only the most important changes are presented and the vibrational degeneracy is ignored. In this Figure we distinguish the largest stretch modes which practically do not change, named *spectator modes* (black line, about 3000 cm^{-1}); the lowest modes corresponding to free rotations and translations in reactants that evolve to vibrations in products, called *transitional modes*; the C-H stretching mode which is broken and transformed in the H-CN stretching mode of the new bond formed, named *reactive mode* (red line) and finally, of special interest in this mechanism of bending excitation, is the change from the bending mode in the ethane reactant (blue line) which evolves to bending mode in the HCN product. We observe that many vibrational modes (with the exception of the spectator and transitional modes) present strong coupling, especially visible in the zone [0-1 bohr] of the reaction coordinate, already in the product zone. Note that s=0 corresponds to the saddle point. However, this does not seem to be the complete picture. The third factor is related with the known QCT limitations due to its classical nature (ZPE violation), and therefore an artificial bending/stretching flux of energy is possible, which would explain the theory/experiment discrepancies in the bending vibrational population. Figure 8 shows this artificial transfer of energy between modes, where the percentage of reactive

trajectories with bending energy, CN stretching energy or CH stretching energy, below its respective ZPE are highlighted. So we observe that 17% of the reactive trajectories appear with bending energy below its ZPE, 32% in the case of the CN stretching energy (which shows that this mode does not conserve the adiabaticity along the reaction) and only 7% in the case of the newly formed CH stretch mode. This artificial transfer of energy could explain, at least partially, the theory/experimental discrepancy about the bending excitation in the HCN product.

Next, we analyse other HCN(v_1, v_2, v_3) populations and compare them with experiment. i) In the present work, we found that the population of the HCN(0,0,0) vibrational ground state is < 1%, reproducing Bethardy et al.'s results for the title reaction, within the theoretical/experimental uncertainties.[4] ii) In addition to the bending excitation, ~80% in the present study, we found hot C-H stretch and cold C-N stretch distributions. Figure 9 presents the distributions of energy deposited in each HCN product degree of freedom, where it can be seen that while the CN stretch mode appears excited by 40%, the CH stretch mode appears excited by 80%. These theoretical results simulate the experimental evidence[4-6] and other theoretical results for the propane reaction.[31] Therefore, given that the reactant CN is in its vibrational ground-state, the CN stretching mode does not behave like a spectator mode, and the excitation of the CH stretching mode can be explained because the motion related to the transfer of the hydrogen atom to the attacking CN radical is very similar to the v_3 normal mode motion in the HCN product (see bottom of Figure 4). iii) Experimentally[4-6] a significant inversion population between HCN(002)-(001) and HCN(001)-(000) was reported. In the present work, the QCT/PES-2023 results reproduce this behaviour: 6.24, 4.19, 0.66% for the HCN(002), (001) and (000), respectively. Finally, iv) the strong inversion of population between HCN(101)-(100) experimentally reported[4-6] was simulated in our calculations, 7.96 and 0.33 %, respectively. In sum, the agreement with the experimental evidence in fine measurements as state-to-state results lends confidence to the theoretical tools used, PES-2023, QCT calculations and NMA analysis.

Finally, other dynamic properties, such as product rotational (PRD), product translational (PTD) and product angular (PAD) distributions, were analysed. Figure 9 (bottom, right panel) shows the HCN rotational distribution at 298 K. The HCN product presents a cold and broad rotational distribution, which is associated with a linear and soft transition state, generating little torque as the reaction evolves. In the same Figure and

panel, PTD is shown at 298 K. Like in the case of PRD, a thermal distribution is found, and both distributions reproduce the experimental evidence.[4-6] Interestingly, similar thermal distributions were reported theoretically by Glowacki et al.[31] for the reaction with propane, and experimentally by Huang et al.[46] for the reactions with n-butane, n-pentane and n-hexane, although it is important to note that different initial conditions were used in these studies. However, in spite of the different conditions in each case, these results seem to suggest a general tendency for the CN + alkane reactions. Finally, the PAD (HCN product with respect to the reactant CN radical) represents another interesting dynamics property. It is given by the differential cross section (DCS), i.e., the variation of the reaction cross section, σ_r with respect to the solid angle (Ω),

$$\frac{d\sigma_r}{d\Omega} = \frac{\sigma_r P(\theta)}{2\pi \sin\theta} \qquad (2)$$

$P(\theta)$ being the product normalized probability of reactive trajectories with angle θ, which is obtained from a histogram analysis by dividing the range [0,180º] into intervals of 10º and counting the number of trajectories per interval. Finally, the Legendre moment method[47] was used to fit the DCS and to smooth this histogram. Figure 10 plots the PADs for the title reaction (solid line) together with the scattering angle for the CN + CH_4 reaction obtained by our group using PES-2017, both at 298 K.[39] Both distributions present a clear backward distribution, associated with a rebound mechanism, clearer in the case of methane reaction. This behaviour is related with the scattering angle/impact parameter relation, i.e., small impact parameters favour backward scattering. While ethane presents a maximum impact parameter of 6.5 Å, the reaction with methane presents a smaller value, 2.6 Å, thus favouring a more backward distribution. As in the cases of PRD and PTD, the PADs simulate previous theoretical[31] and experimental[46] backward distributions in other alkanes (from propane to hexane), although as was previously noted, the initial conditions were different. Again, these results suggest a general tendency in the CN + alkane reactions. Before finishing this Section, we consider the evolution of the DCSs with temperature (equivalent to the initial collision energy). Figure 11 shows the scattering distributions from 25 to 1000 K (equivalent to initial average collision energies from 0.03 to 2.80 kcal mol^{-1}). QCT results show a dramatic transition from forward-backward distributions at low temperatures (25-200 K), associated with an indirect complex-forming mechanism, to backward-dominated DCSs at intermediate temperatures (300-500 K), associated with a direct rebound mechanism,

and finally, a practically isotropic DCS at the highest temperature (1000 K), with a predominance of sideways scattering. In order to explain the DCS behaviour, several factors should be considered: i) maximum impact parameter, b_{max}, which decreases as temperature increases, from 10.0 Å to 5.5 Å in the range 25-1000 K. It is known that low b_{max} are associated with backward scattering and rebound mechanisms, while high b_{max} are associated with forward scattering and stripping mechanisms; ii) influence of the reactant complex, more important at lower temperatures, and iii) influence of the product complex, which causes the initial orientation of the prodcuts to be "forgotten". It is known that the presence of intermediate complexes favours isotropic distributions and forward-backward distributions. The final DCS result indicates the balance of a complicated interplay of several factors.

Finally, the present results were compared with related halogen and oxygen reactions, because the CN radical can be considered as a pseudohalogen with similar reactivity and electron afinity, 3.82 eV versus 3.60 eV for F and Cl atoms:[48,49]

$$X + C_2H_6 \rightarrow XH + C_2H_5, \qquad X \equiv CN, F, Cl, O(^3P)$$

with the difference in the XH product, diatomic for F, Cl and $O(^3P)$ and triatomic for CN. The reactions of F, Cl and $O(^3P)$ have been widely studied and our group developed the respective analytical full-dimensional PESs between 2017 and 2020 (Refs. 50-56 and references therein). A summary of theoretical results[50-56] is shown in Table 2, the attacking species in function of exothermicity being presented in order. Note that different initial conditions were used in each reaction and that this comparison is merely a guide of behaviour. This exothermicity decreases in the order F > CN > Cl > O and related with this variation the barrier height increases in the same order, following Hammond's postulate.[57] With these barriers, very fast reactions and a negligible tunnelling effect is expected for the F and CN reactions, and lower rate constants and an increase of the tunnelling factor are expected for the Cl and O reactions. For the F and CN reactions the transition state is located "early" on the reaction path and therefore substantial product vibrational excitation is found, 66 and 65%, respectively, of the available energy. This product vibrational excitation decreases for the Cl and O reactions, increasing the translational fraction. With respect to product vibrational distribution, which is one of the aims of the present paper, the situation is very different for the diatomic and triatomic products. While the diatomic products, FH(v), ClH(v) and OH(v),

presented few populated vibrational states, with the ClH(v) and OH(v) products practically in their respective vibrational ground-states, the HCN(v) presented many populated states with a low population in each one, with bending and stretching excitations. The product scattering distribution shows a clear evolution from forward to backward scattering in the order F, CN, Cl and O, related mainly with the decreases of the impact parameter in the series. In general, high impact parameters favour forward scattering and stripping mechanisms, while low impact parameters favour backward distributions and rebound mechanisms.

5. CONCLUSIONS

The CN + C_2H_6 hydrogen abstraction gas-phase reaction represents a ten-body polyatomic complex system with 24 degrees of freedom. To describe the nuclear motion an analytical full-dimensional potential energy surface, PES-2023, was developed as a combination of valence bond and molecular mechanics functions, and fitted to high level *ab initio* calculations at the CCSD(T)-F12/aug-cc-pVTZ level. As these functions are based on simple and physically intuitive ideas, stretching, bending, torsions, etc, they permit i) the transferability from previous and similar surfaces to a new one, and ii) the use of a reduced and selected number of *ab initio* calculations in the fitting process, which represents an important saving of computational time and an advantage with respect to other approaches. PES-2023 simulates the *ab initio* enthalpy of reaction, barrier height and stability of the complexes in the entrance and exit channels, describing the topology of the surface for the electronic ground-state, within the Born-Oppenheimer approximation. This agreement represents a first test of quality of the new surface.

Based on PES-2023 a dynamics analysis was carried out using QCT calculations at a temperature of 298 K for a direct comparison with experiments, focussing attention on the well-studied HCN(v_1,v_2,v_3) product. It was found that the largest fraction of energy available was deposited as HCN vibrational energy, ~ 65%, and that the HCN product vibrational population was inverted in the CH stretching mode and not inverted in the CN stretching and bending modes. PES-2023 reasonably reproduces these experimental findings, which represents a second test of confidence of the tools used, PES-2023, QCT and the NMA method. We suggest that coupling and transfer of energy between modes immediately after HCN formation, associated with the classical nature of the QCT results,

could explain the lower bending vibrational populations as compared to the experimental findings.

In order to complete the dynamics study, the product rotational, translational and angular distributions were analysed at room temperature. We found thermal distributions for the rotation and translation distributions and backward scattering, associated with a rebound mechanism.

In sum, several tests showed that PES-2023 presents great versatility and capacity to describe the dynamics behaviour of this ten-body polyatomic system. In addition, it should be noted that PES-2023 can also be used in kinetics studies, which will be addressed in the near future.

ACKNOWLEDGEMENTS

The authors gratefully acknowledge the computer resources at Lusitania (COMPUTAEX) and technical support provided by Felipe Lemus. We are grateful to James McCue for assistance in language editing.

REFERENCES

(1) J. C. Polanyi, *Acc. Chem. Res*. **5**, 161 (1972).

(2) J. C. Polanyi, and J. L. Schreiber, *Physical Chemistry: An Advanced Treatise*, Vol. 6A, edited by W. Jost Academic, New York, 1974.

(3) R. D. Levine, and R. B. Bernstein, *Molecular Reaction Dynamics and Chemical Reactivity*, Oxford, Oxford, 1987.

(4) G. A. Bethardy, F. J. Northrup, and R. G. Macdonald, *J.Chem.Phys*. **102**, 7966 (1995).

(5) L. R. Copeland, F. Mohammad, M. Zahedi, D. H. Volman, and W. M. Jackson, *J.Chem.Phys*. **96**, 5817 (1992).

(6) V. R. Morris, F. Mohammad, L. Valdry, and W. M. Jackson, *Chem.Phys.Lett*. **220**, 448-454 (1994).

(7) G. Herzberg, Molecular Spectra and Molecular Structure volume II, Infrared and Raman Spectra of Polyatomic Molecules (Van Nostrand Reinhold Company, New York, 1945).

(8) Y.L. Lung, M. Allen, and J.P. Pinto, *Astrophys. J. Suppl. Ser*. **55**, 465 (1984).

(9) E. Herbert, and W. Klemperer, *Astrophys. J.* **185**, 505 (1973).

(10) Y.P. Viala, *Astron. Astrophys. Suppl. Ser*. **64**, 391 (1986).

(11) L. Herbert, I.W.M. Smith, and R.D. Spencer-Smith, *Intern. J. Chem. Kinetics* **24**, 791 (1992).

(12) J. A. Miller, and C. T. Bowman, *Prog. Energy Combust. Sci*. **15**, 287 (1989).

(13) B. Ruscic, R. E. Pinzon, G. von Laszewski, D. Kodeboyina, A. Burcat, D. Leahy, D. Montoy, and A. F. Wagner, *J. Phys.: Conf. Ser*. **16**, 561–570 (2005); B. Ruscic, *J. Phys. Chem. A* **119**, 7810–7837 (2015).

(14) NIST Chemical Kinetics Database web page. Standard References Database 17, Version 7.0 (Web Version), Release 1.6.8. Data Version 2015.09

(15) Y. Georgievskii, and S.J. Klippenstein, *J.Phys.Chem. A*, **111**, 3802-3811 (2007).

(16) M. J. Frisch et al., Gaussian 16, Revision C.01, Gaussian, Inc., Wallingford, CT, 2016.

(17) H.J. Werner et al., MOLPRO, version 2015.1, a package of *ab initio* programs, 2015, see http://www.molpro.net.

(18) T.J. Lee, A.P. Rendell, and P.R. Taylor, *J. Phys. Chem.* **94**, 5463 (1990).

(19) J. Lee, and R. Taylor, *Int. J. Quantum Chem*., **36**, 199-207 (1989).

(20) C. Rangel, J.C. Corchado, and J. Espinosa-Garcia, *J.Phys.Chem. A*, **110**, 10375-10383 (2006).

(21) J. Espinosa-Garcia, and J.C. Corchado, *Theor.Chem.Acc*. 134:6 (2015).

(22) C. Rangel, M. Garcia-Chamorro, J.C. Corchado, and J. Espinosa-Garcia, *Phys. Chem. Chem. Phys*. **22**, 14796-14810 (2020).

(23) J. Espinosa-Garcia, and J.C. Corchado, *Phys. Chem. Chem. Phys*. **23**, 21065-21077 (2021).

(24) C. Rangel, J. Espinosa-Garcia, ad J.C. Corchado, *Phys. Chem. Chem. Phys*. **24**, 12501-12512 (2022).

(25) J. Espinosa-Garcia, C. Rangel, and Y.V. Suleymanov, *Phys.Chem.Chem.Phys*. **19**, 19341-19351 (2017).

(26) J.C. Corchado, J.L. Bravo, and J. Espinosa-Garcia, *J.Chem.Phys*. **130**, 184314 (2009).

(27) Y. Shu, Z. Varga, A.W. Jasper, B.C. Garrett, J. Espinosa-García, J.C. Corchado, R.J. Duchovic, Y.L. Volobuev, G.C. Lynch, K.R. Yang, T.C. Allison, A.F. Wanger, and D.G. Truhlar, POTLIB, http://comp.chem.umn.edu/potlib.

(28) R.J. Duchovic, Y.L. Volobuev, G.C. Lynch, D.G. Truhlar, T.C. Allison, A.F. Wanger, B.C. Garrett, and J.C. Corchado, POTLIB: A Potential Energy Surface

Library for Chemical Systems. *Comput. Phys. Commun*. **144**, 169-187 (2002); **156**, 319-322 (2004) (E).

(29) Y. Zhao, and D. G. Truhlar, *J. Chem. Theory Comput*., **4**,1849–1868 (2008).

(30) B. J. Lynch, Y. Zhao, and D. G. Truhlar, *J. Phys. Chem. A*, **107**, 1384 (2003).

(31) D.R. Glowacki, A. Orr-Ewing, and J.N. Harvey, *J.Chem.Phys*. **134**, 214508 (2011).

(32) X. Hu, W.L. Hase, and T. Pirraglia, *J.Comput.Chem*. **12**, 1014 (1991).

(33) W.L. Hase, R.J. Duchovic, X. Hu, A. Komornicki, K.F. Lim, D-h. Lu, G.H. Peslherbe, K.N. Swamy, S.R. Vande Linde, A.J.C. Varandas, H. Wang, and R.J. Wolf, VENUS96: A General Chemical Dynamics Computer Program, QCPE Bull. **16**, 43 (1996).

(34) J.C. Corchado, and J. Espinosa-Garcia, *Phys.Chem.Chem.Phys*. **11**, 10157-10164 (2009).

(35) L. Bonnet, *J Chem Phys* **128 ,** 044109 (2008)

(36) L. Bonnet, *Int Rev Phys Chem* **32,** 171-228 (2013)

(37) G. Czako, and J.M. Bowman, *J Chem Phys* **131**, 244302 (2009).

(38) L. Bonnet, and J. Espinosa-Garcia, *J Chem Phys* **133**, 164108 (2010).

(39) J. Espinosa-Garcia, and J. Garcia-Bernaldez, *Theor.Chem.Acc*. **136**,121 (2017)

(40) E. Garcia, J.C. Corchado, and J. Espinosa-Garcia, *J Comput Theor Chem* **990,** 47-52 (2012)

(41) J.C. Corchado, J. Espinosa-Garcia, J. Li, and H. Guo, *J.Phys.Chem. A*, **117**, 11648-11654 (2013).

(42) L. Bonnet J. Espinosa-García, J.C. Corchado, S. Liu, and Dong H. Zhang, *Chem.Phys.Lett*., **516**, 137-140 (2011).

(43) G. A. Bethardy, F. J. Northrup, and R. G. Macdonald, *J.Chem.Phys*. **105**, 4533 (1996).

(44) J. Espinosa-Garcia, M. Garcia-Chamorro, and J.C. Corchado, *Theor.Chem.Acc*. **139**, 63 (2020).

(45) B. Nizamov, D.W. Setser, H.B. Wang, G.H. Peslherbe, and W.L. Hase, *J. Chem. Phys.* **105**, 9897 (1996)

(46) C. Huang, W. Li, A. D. Estillore, and A. G. Suits, *J.Chem.Phys*. **129**, 074301 (2008).

(47) D.G. Truhlar, and N.C. Blais, *J Chem Phys* **67**, 1532-1539 (1977).

(48) R. D. Mead, A. E. Stevens, and W. C. Lineberger, *Gas-Phase Ion Chemistry*, Vol. 3, edited by M. T. Bowers Academic, New York, 1984.

(49) P. S. Drzaic, J. Marks, and J. I. Braumann, *Gas-Phase Ion Chemistry*, Vol. 3, edited by M. T. Bowers Academic, New York, 1984.

(50) J. Espinosa-Garcia, J. C. Corchado, M. Garcia-Chamorro, and C. Rangel, *Phys.Chem.Chem.Phys*., **20**, 19860 (2018).

(51) J. Espinosa-Garcia, and M. Garcia-Chamorro, Phys.Chem.Chem.Phys., **20**, 26634 (2018).

(52) C. Rangel, and J. Espinosa-Garcia, *Phys.Chem.Chem.Phys*., **20**, 3925 (2018).

(53) J. Espinosa-Garcia, E. Martinez-Nuñez, and C. Rangel, *J. Phys. Chem. A*, **122**, 2626−2633 (2018).

(54) J.C. Corchado, M. Garcia-Chamorro, C. Rangel, and J. Espinosa-Garcia, *Theoretical Chemistry Accounts*, **138**, 26 (2019).

(55) J. Espinosa-Garcia, C. Rangel, J. C. Corchado, and M. Garcia-Chamorro, *Phys.Chem.Chem.Phys.*, **22**, 22591 (2020).

(56) M. Garcia-Chamorro, J. C. Corchado, and J. Espinosa-Garcia, *Theoretical Chemistry Accounts*, **139**, 182 (2020).

(57) G.S. Hammond, *J.Am.Chem.Soc*., **77**, 334 (1955).

Table 1. Properties[a] for the CN + CH_4 (PES-2017)[25] and CN + C_2H_6 (present PES-2023) reactions.

Property	CN + CH_4 [b]	CN + C_2H_6 [c]
Geometry		
C-H´	1.182 (8%)[d]	1.113 (2%)
H´-CN	1.745 (60%)	1.793 (67%)
C-H´-CN	180.0	180.0
Imaginary frequency		
ω_i	350	150
Energy		
$\Delta E^{\neq}$	2.5	0.23
ΔE_R	-20.0	-22.2
RC	-0.1	-0.27
PC	-0.8	-1.10

a) Geometry: distances in Å and angle in degrees. Vibrational frequency in cm^{-1}. $\Delta E^{\neq}$, ΔE_R, RC and PC are, respectively, classical barrier height, classical reaction energy, reactant complex stability with respect to the reactants and product complex stability with respect to the products, in kcal mol^{-1}

b) CN + CH_4 reaction using the PES-2017.[25]

c) Present work using the PES-2023.

d) In parentheses, increase in percentage with respect to reactant or product.

Table 2. Comparison of properties for X + C_2H_6 reactions, X≡F, CN, Cl, O(^{3}P)

Property	**F(^{2}P)[h]**	**CN(X $^2\Sigma^+$)[i]**	**Cl(^{2}P)[j]**	**O(^{3}P)[k]**
Reaction energy	-31.60	-22.20	+1.82	+2.22
Barrier height	+0.15	+0.23	+2.44	+10.70
Complexes[a]	yes	yes	yes	yes
$<f_V>^{XH\ b}$	0.66	0.65	0.16	0.25
$<f_T>^c$	0.17	0.10	0.47	0.44
PVD[d]	FH(0,1,2,3) 0:2:58:40	*Many populated states *Bending and stretching excitations	ClH(0,1) 97:3	OH(0,1) 98:2
PAD[e]	Sideways-forward	Sideways-backward	Sideways-backward	Backward
b_{max} [f]	4.0	6.5	3.5	2.9
k(298 K)[g]	$1.03x10^{-10}$	$1.92x10^{-11}$	$2.41x10^{-11}$	$9.14x10^{-16}$

a) Existence of intermediate complexes in the entrance and exit channels
b) Fraction of energy as XH(v) product vibration
c) Fraction of energy as translation
d) Product vibrational distribution
e) Product angular distribution
f) Impact parameter maximum, in Å
g) Rate constants, in cm^3 $molecule^{-1}$ s^{-1} using variational transition state theory
h) Using PES-2018 at fixed collision energy of 3.2 kcal mol^{-1} (Refs. 50,51)
i) Using PES-2023 at room temperature (present work)
j) Using PES-2017 at fixed collision energy of 5.5 kcal mol^{-1} (Refs. 52-54)
k) Using PES-2020 at fixed collision energy of 7.0 kcal mol^{-1} (Refs. 55, 56)

FIGURE CAPTIONS

Figure 1. Schematic classical energy diagram of the stationary points for the CN + C_2H_6 gas-phase reaction. PES-2023 results in blue and CCSD(T)-F12/aug-cc-pVTZ *ab initio* level in red. As insert, the optimized geometries of the reactant complex, (here, in the RC the upper figure corresponds to the PES-2023 while the lower figure corresponds to the CCSD(T)/cc-pVTZ level), saddle point and product complex are included.

Figure 2. Potential energy curves (in kcal mol^{-1}) as a function of the reaction coordinate (in bohr) with respect to the reactants. Note that the value zero in the reaction coordinate corresponds to the saddle point and positive/negative values correspond, respectively, to product/reactant channels. PES-2023 (solid line), CCSD(T)-F12/aug-cc-pVTZ//MP2 (dashed line).

Figure 3. Contour plots showing the broken and formed bonds, C-H' and H'-CN, respectively, while the remaining coordinates are fixed at their values in the saddle point, and are denoted by a cross. Upper panel: CN + ethane reaction using PES-2023. Lower panel: CN + methane reaction using PES-2017.[25]

Figure 4. Schematic energetic profile of the CN + $C_2H_6 \rightarrow HCN(v_1,v_2,v_3) + C_2H_5$ reaction using the PES-2023 surface. The pure vibrational states of the HCN product are included, which are labelled (n_{CN}, $n_{bending}$, n_{CH}). The vibrational modes are shown below the level diagram.

Figure 5. QCT/PES-2023 bending vibrational distributions at 298K for the HCN(v_1,v_2,v_3) states where all co-product states are considered.

Figure 6. Variation of the energy with the bending motion of the saddle point (NC-H'-R) for the CN + C_2H_6 reaction using PES-2023 (present work, solid line) and for the CN + CH_4 reaction using PES-2017 (dashed line),[25] taking as reference the respective equilibrium geometry, 180º. Note that the remaining parameters at the respective saddle points were kept at the reference system.

Figure 7. Generalized normal-mode vibrational frequencies (in cm^{-1}) as a function of the reaction coordinate, *s* (bohr), for the CN + C_2H_6 reaction using PES-2023. Values $s < 0$ correspond to reactants and values $s > 0$ to products.

Figure 8. HCN product energy in the different modes (bending, CN stretching and CH stretching) from QCT calculations using PES-2023. The horizontal and vertical black lines represent ZPE violation for the modes. Energies in kcal mol^{-1}.

Figure 9. Distributions of energy deposited in each HCN product degree of freedom, vibration, rotation and translation.

Figure 10. Product angular distributions at 298 K for the ethane reaction using the PES-2023 surface (solid line) and for the methane reaction using the PES-2017 surface (dashed line).[25] Note that all products are considered, irrespective of their internal energy.

Figure 11. Product angular distributions at different temperatures for the title reaction, normalized to unity for a clearer comparison.

FIGURE 1

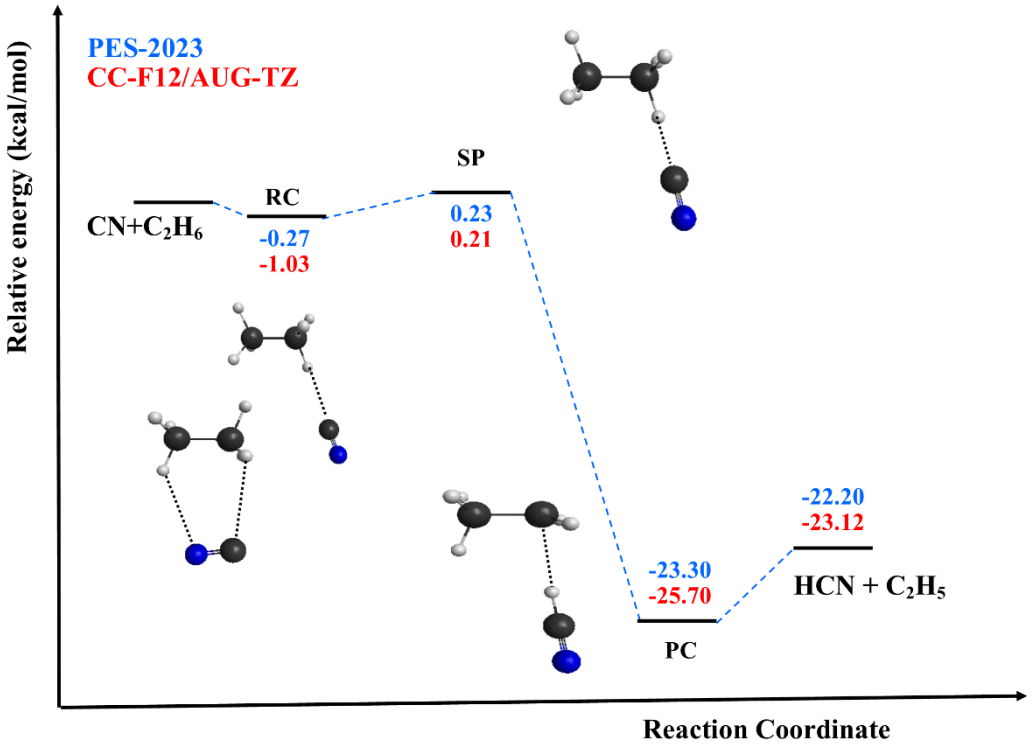

FIGURE 2

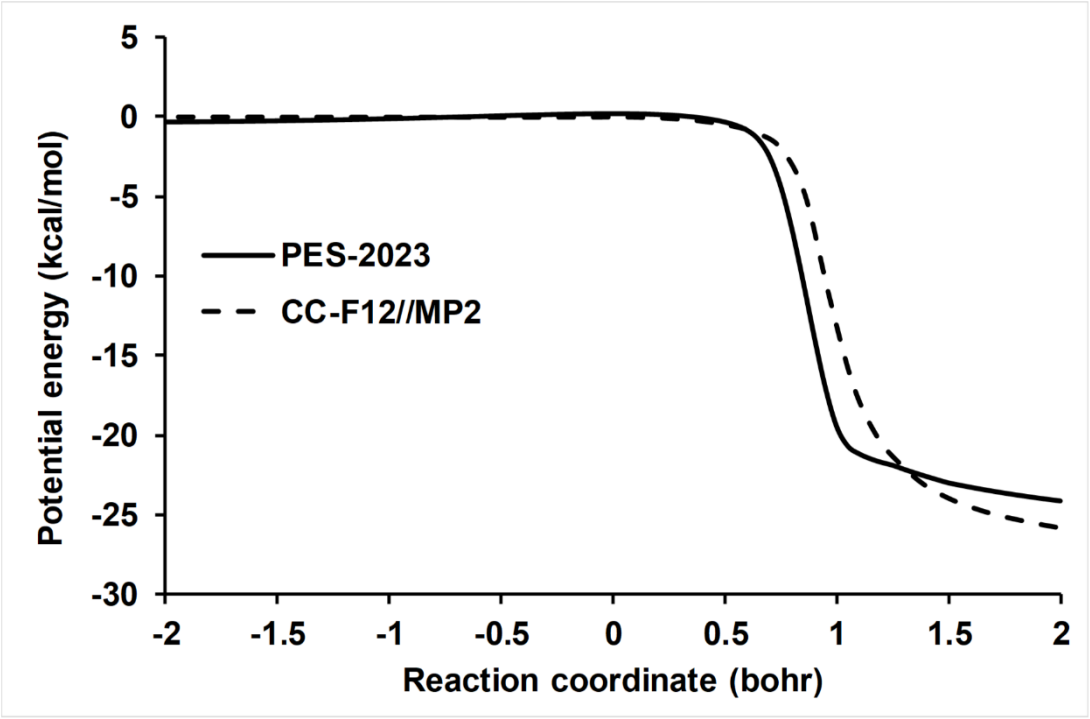

FIGURE 3

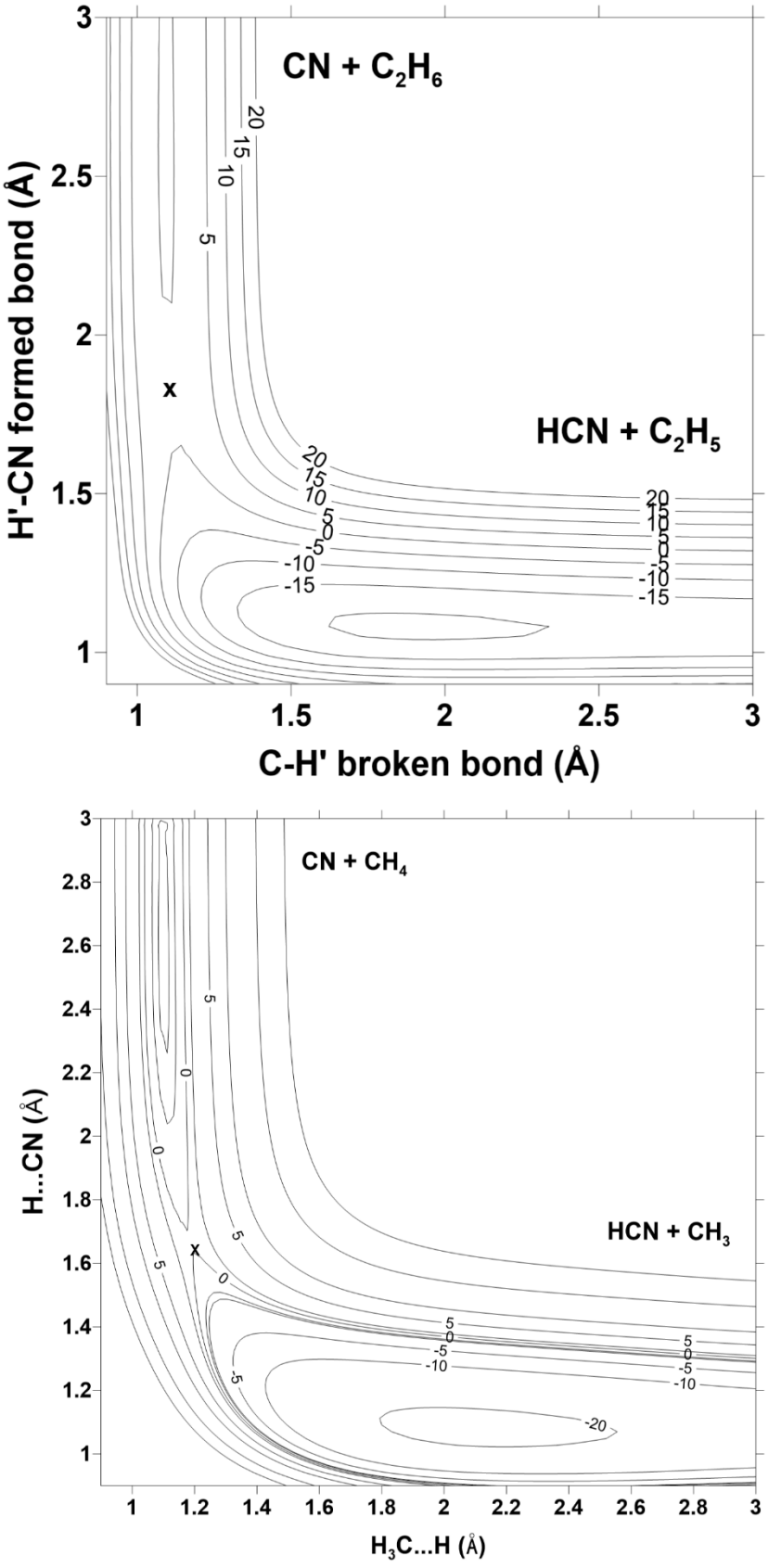

FIGURE 4

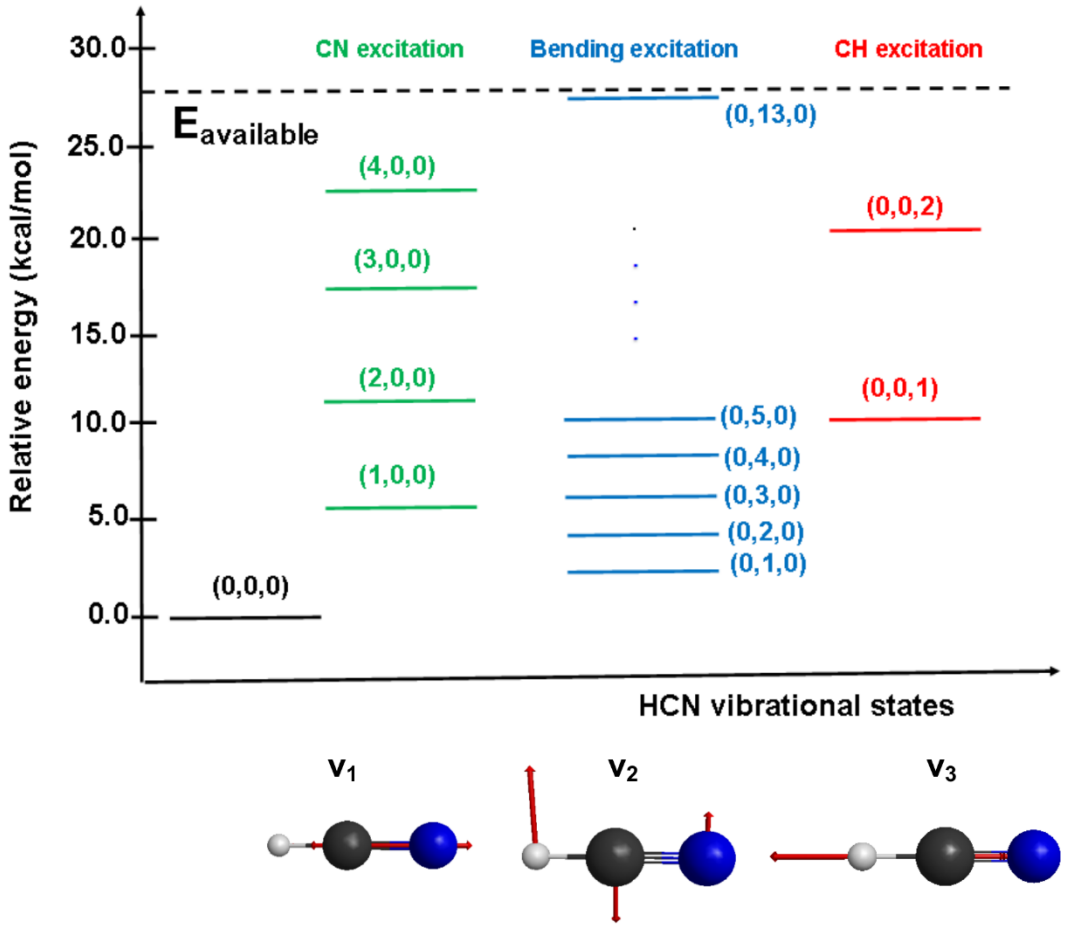

FIGURE 5

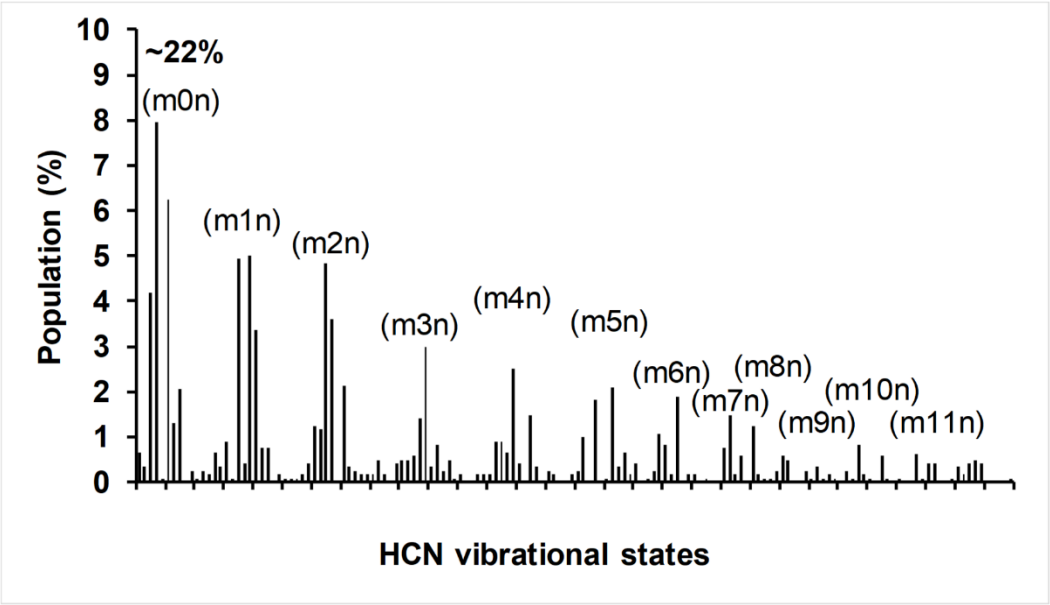

FIGURE 6

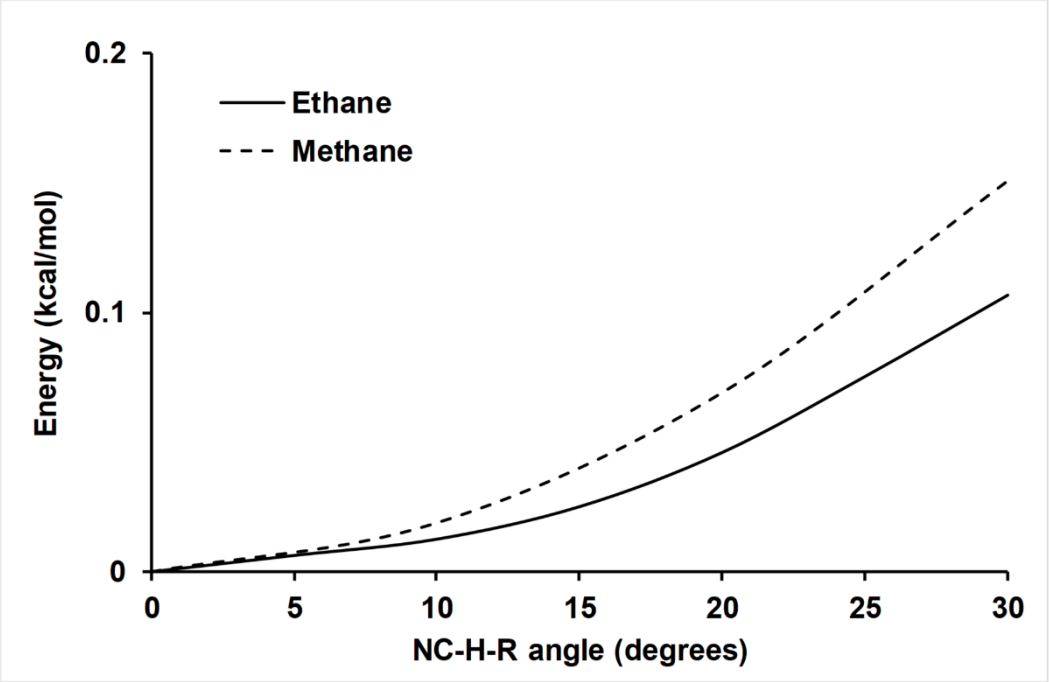

FIGURE 7

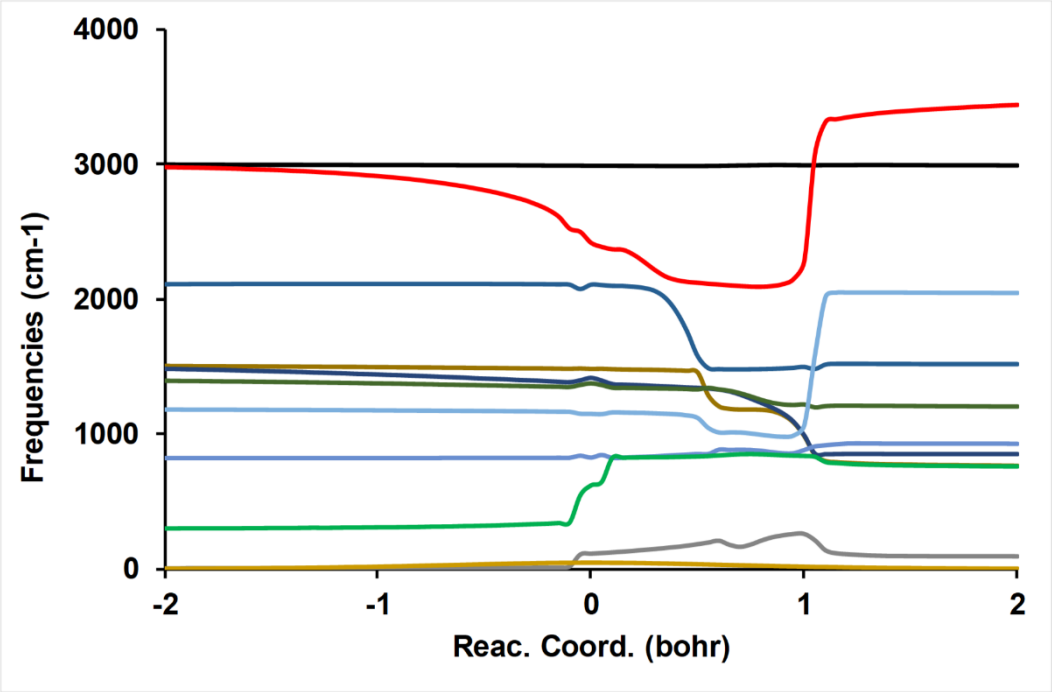

FIGURE 8

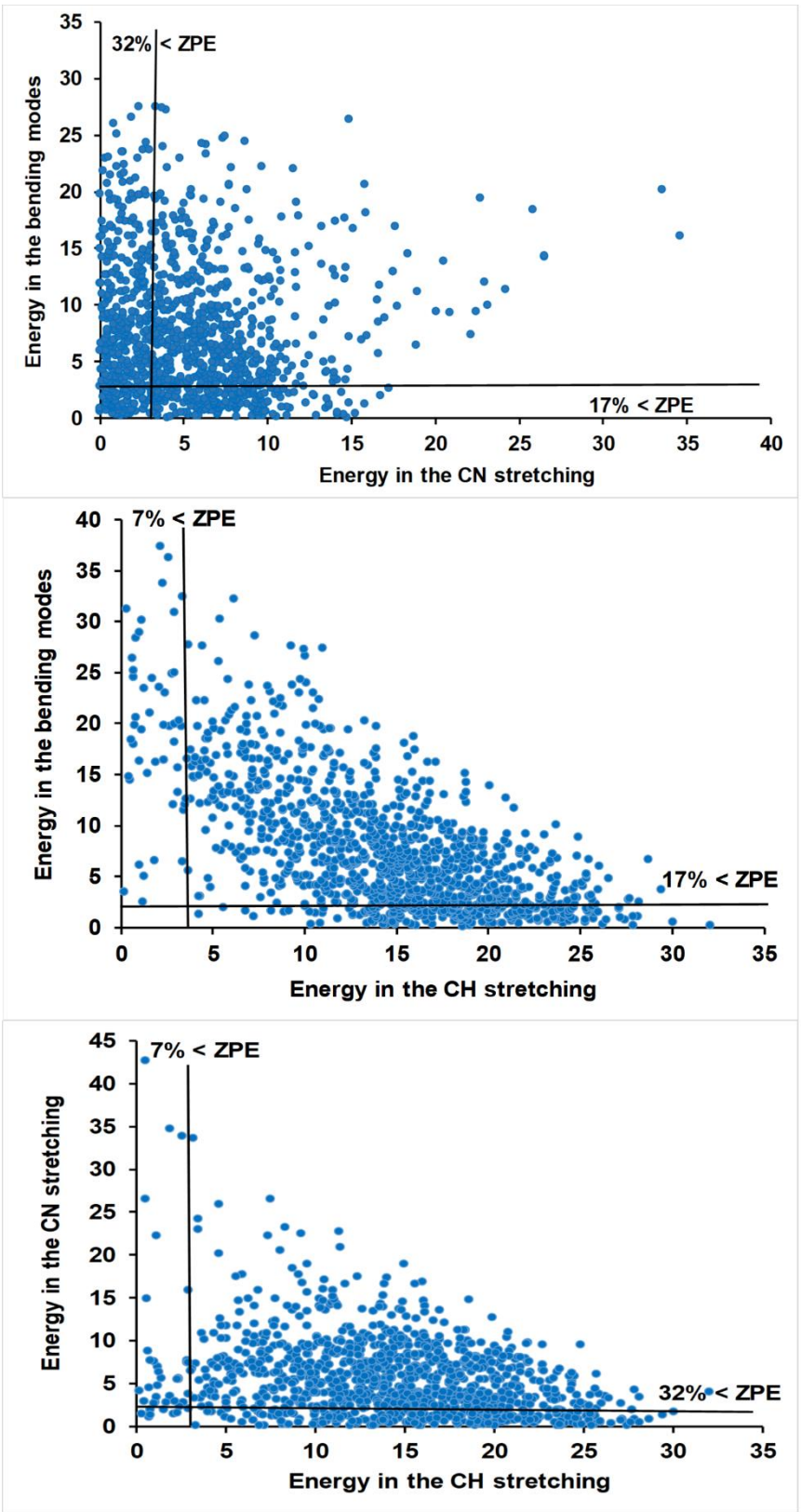

FIGURE 9

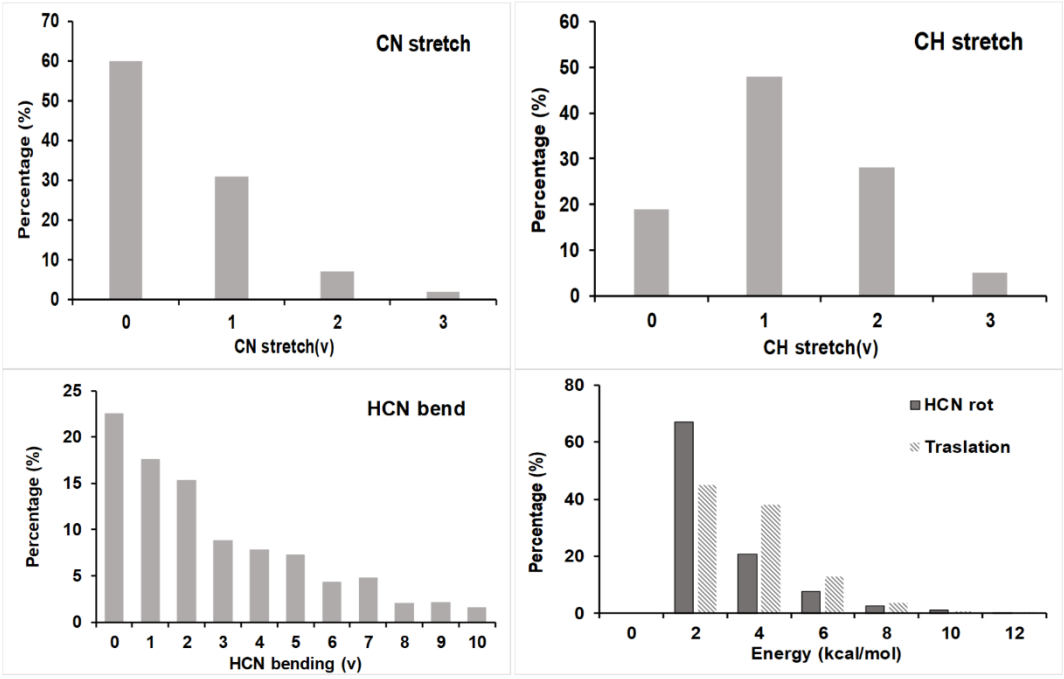

FIGURE 10

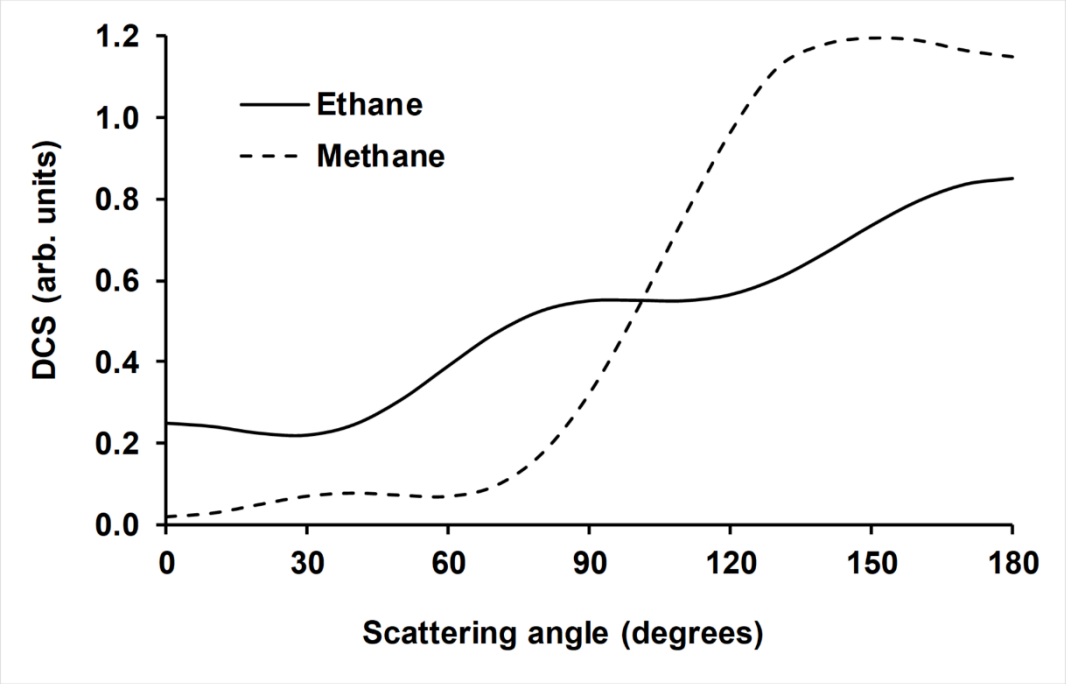

FIGURE 11